Introduction to HOBIT, a b-Jet Identification Tagger at the CDF Experiment Optimized for Light Higgs Boson Searches

J. Freeman[a], T. Junk[a], M. Kirby[a,1], Y. Oksuzian[b], T.J. Phillips[c], F.D. Snider[a], M. Trovato[e], J. Vizan[f], W.M. Yao[d]

[a] *Fermi National Accelerator Laboratory, Batavia, IL, 60510, USA*
[b] *Univeristy of Virginia, Charlottesville, Virginia, 22906, USA*
[c] *Duke University, Durham, North Caronlina, 27708, USA*
[d] *Ernest Orlando Lawrence Berkeley National Laboratory, Berkeley, California, 94720, USA*
[e] *Isituto Nazionale di Fisica Nucleare Pisa, Scuola Normale Superiore, I-56127 Pisa, Italy*
[f] *Université catholique de Louvain, Louvain la Neuve, B-1348, Belgium*

Abstract

We present the development and validation of the Higgs Optimized b Identification Tagger (HOBIT), a multivariate b-jet identification algorithm optimized for Higgs boson searches at the CDF experiment at the Fermilab Tevatron. At collider experiments, b taggers allow one to distinguish particle jets containing B hadrons from other jets; these algorithms have been used for many years with great success at CDF. HOBIT has been designed specifically for use in searches for light Higgs bosons decaying via $H \to b\bar{b}$. This fact combined with the extent to which HOBIT synthesizes and extends the best ideas of previous taggers makes HOBIT unique among CDF b-tagging algorithms. Employing feed-forward neural network architectures, HOBIT provides an output value ranging from approximately -1 ("light-jet like") to 1 ("b-jet like"); this continuous output value has been tuned to provide maximum sensitivity in light Higgs boson search analyses. When tuned to the equivalent light jet rejection rate, HOBIT tags 54% of b jets in simulated 120 GeV/c^2 Higgs boson events compared to 39% for SecVtx, the most com-

☆FERMILAB-PUB-12-118-PPD

*Corresponding author
Email address: kirby@fnal.gov (M. Kirby)

monly used b tagger at CDF. We present features of the tagger as well as its characterization in the form of b-jet finding efficiencies and false (light-jet) tag rates.

Keywords: b-jet identification, b-tagging, standard model Higgs boson, CDF, Tevatron

1. Introduction

At CDF, the search for a light Higgs boson has been a subject of increasing interest and focus in recent years. While there have been numerous successful b-jet identification algorithms (commonly referred to as "b taggers") over the years, most have been intended for use in analyses other than searches for $H \to b\bar{b}$. Aspects of a given analysis, however, such as the optimal signal-to-background ratio, or the relative rate of non-b jets originating from gluons in the data sample before tagging, can influence whether a tagger is optimal for the analysis in question. Traditional taggers have tended toward a higher purity and lower efficiency than would be ideal for Higgs boson searches given the relatively low cross section of Higgs boson production at Tevatron energies. While this problem has been circumvented somewhat by taking the logical OR of several taggers, a more elegant and flexible solution can be found in the continuous output of a neural network, tunable for each analysis application.

In this paper, we describe the Higgs Optimized b Identification Tagger (HOBIT). The strategy used in developing HOBIT is to build upon the strengths of previous CDF b taggers, address their weaknesses, and construct a new tagger that is highly optimized specifically for finding light Higgs boson decays. HOBIT produces a continuous output variable, allowing efficiency and background rejection to be tuned to meet the requirements of a given search. In the next section, we review some of the general features of b quark decays used by HOBIT to distinguish jets containing B hadrons from jets produced by gluons or light quarks (up, down, or strange). Section 3 then describes some of the previous b-tagging algorithms used by CDF upon which HOBIT is built. We then discuss some features of the CDF detector in Sec. 4, followed by a detailed description of the HOBIT algorithm and training regimen. The performance of HOBIT as characterized by the b-jet tagging efficiency and background rejection rates in data and Monte Carlo (MC) is presented in Sec. 6. We conclude in Sec. 7.

2. Physics of *b*'s from Higgs Boson Decay

Jets containing high-E_T B hadrons such as are created in a light Higgs boson decay possess several features that distinguish them from jets produced by light quarks or gluons. The most important of these is the relatively long lifetime of a B hadron, augmented in the lab frame by its relativistic boost, which allows it to travel a distance on the order of a millimeter[1]. The B hadron's travel across these macroscopic distances results in a displacement between the location of the $p\bar{p}$ collision (the "primary" vertex) and the B hadron decay (the "secondary", or "displaced" vertex). These displacements are resolvable by the CDF tracking system, and in particular by its silicon detector. Almost all information as to whether or not a given jet originates from b-quark production is carried in the tracks reconstructed from detector signals left by the jet's charged particles. Specifically, it is possible to identify the decay of a B hadron through the displacement from the primary vertex of the individual tracks it leaves in the detector, and also through the displacement of a B-hadron decay vertex formed by combining multiple displaced tracks in a fit.

Other features also distinguish the b jet from other jets. Due to the large mass of the b quark, the collective invariant mass of the decay products of B hadrons will be larger than those from the decay products of hadrons not containing b quarks. Furthermore, the large relativistic boost typical of a B hadron will result in decay products which tend to be more energetic and collimated within a jet cone than other particles. Finally, particle multiplicities tend to be different for jets containing B hadron decays compared to other jets; in particular, muons or electrons appear in approximately 20% of jets containing a B hadron, either directly via semileptonic decay of the B or indirectly through the semileptonic decay of charm hadrons resulting from a B decay.

3. *b*-Tagging Algorithms

As a tremendous amount of effort has gone into the construction of b taggers at CDF and other experiments [1, 2, 3], we build upon previous experience when constructing HOBIT. In particular, HOBIT explicitly uses

[1] This distance is achieved due to the fact that c times the rest frame lifetime of a B^0 ($B^{\pm}$, B_s, Λ_b) hadron is 460 μm (501 μm, 441 μm, 367 μm).

as inputs the output of the SecVtx algorithm set to its "loose" operating point [4], the output of CDF's soft muon tagger [5], and inputs to the earlier RomaNN [6, 7] and Bness [8] multivariate taggers. Consequently, it is useful to describe these taggers.

3.1. SecVtx

SecVtx is a displaced vertex tagger and the most commonly used b tagger at CDF. SecVtx only uses tracks which are significantly displaced from the primary vertex, accepted by quality requirements, and within a distance of $\Delta R < 0.4$ of the jet axis. Here, $\Delta R = \sqrt{\Delta\phi^2 + \Delta\eta^2}$, where ϕ is the azimuthal angle of the track around the beam axis, and η is its pseudorapidity defined as $\eta = -\log(\tan(\frac{\theta}{2}))$, with θ the polar angle of the track with respect to the beam axis. With these tracks, SecVtx uses an iterative method to fit a displaced vertex within the jet, where the χ^2 of the vertex fit is employed to guide the process. Assuming that this displacement is due to the long lifetime of the B hadron, the significance of the two-dimensional decay length L_{xy} in the plane perpendicular to the beampipe axis is used to select b-jet candidates. The algorithm is utilized with different track requirements and threshold values in order to achieve different efficiencies and purity rates. In practice, three operating points are used, referred to as "loose", "tight", and "ultra-tight". The loose SecVtx operating point decision is used as an input to both the RomaNN and HOBIT tagger. One drawback of the SecVtx tagger is that it is unable to fit a vertex in every b jet. In the Pythia [9] 120 GeV/c^2 Higgs boson Monte Carlo (MC) whose b jets are used to train HOBIT, SecVtx operating at its "loose" setting fails to find a vertex in 44.3% of these jets.

3.2. Soft Lepton Taggers

Soft lepton taggers [5] (SLT) take a different approach to b tagging. Rather than focusing on tracks within a jet, they select B hadron decays by identifying charged leptons inside a cone around the jet axis. Since the b semileptonic branching ratio is approximately 10% per lepton flavor, this class of tagger is not competitive with SecVtx or the other taggers described below if used alone. However, because a soft lepton tagger does not rely on the presence of displaced tracks or vertices, it has a chance to identify b jets that the other methods cannot. In practice, CDF uses only a soft muon tagger since high-purity electron or τ identification within jets is difficult. HOBIT uses as inputs the number of soft muon tags within a jet as well as the momentum transverse to the jet axis of the muon with the highest-likelihood tag.

3.3. The RomaNN Tagger

The "RomaNN tagger" has been used at CDF in light Higgs boson searches [6, 7] and employs neural network architectures. Neural networks (NNs) can use as many flavor-discriminating observables as is computationally feasible; hence the efficiency of NN taggers is equal to or greater than that of conventional taggers for a given purity. While the SecVtx tagger attempts to find exactly one displaced vertex in a jet, the RomaNN tagger uses a vertexing algorithm that can find multiple vertices, as may be the case when multiple hadrons decay within the same jet cone (for example, in a $B \to D$ decay). The RomaNN tagger uses several types of NNs: one to distinguish vertices which come from a heavy flavor (B or charm) hadron from false vertices or vertices coming from other hadrons; another to identify unvertexed tracks which come from a heavy flavor hadron; and then another NN which takes as inputs the output of the first NNs along with other inputs, including the loose SecVtx tag status, the number of SLT-identified muons, and the vertex displacement and mass information. Distinct versions of this third NN are trained to separate b jets from light jets, charm jets from light jets, and b jets from charm jets; the outputs of these three flavor-separating NNs are then used to train a final NN whose output is the RomaNN discrimination variable. The RomaNN tagger not only has superior performance to that of SecVtx at equivalent purities (see Fig. 5), but also allows for an "ultra-loose" operating point yielding greater efficiency, particularly useful in light Higgs boson searches.

However, the RomaNN tagger is not guaranteed to fit a vertex or to have sufficient input information to reliably tag a jet. In the event that the RomaNN tagger fails to receive sufficient information from its inputs, it is unable to assign an output value to that jet. This is the case with 20.6% of the b jets in the aforementioned light Higgs boson MC sample. Regardless, due to the usefulness of the RomaNN inputs, a majority of them are employed as inputs into the HOBIT tagger, which allows HOBIT to take advantage of the same extensive vertex information that the RomaNN tagger uses.

3.4. The Bness Tagger

While the RomaNN tagger focuses on the vertices it finds within a jet, in the event that it is unable to fit any vertices, it is unable to distinguish b jets from light jets. However, a significant proportion of b jets (approximately 20% in Higgs boson candidate events) do not contain a sufficient number of well-reconstructed tracks to allow for a vertex fit in the RomaNN tagger. The Bness tagger [8] uses not only vertex information within a jet, but also the properties of individual tracks to determine whether a jet is b-like. (The RomaNN tagger only examines individual tracks based on their proximity to a displaced vertex). To evaluate the information from individual tracks, the Bness tagger utilizes an NN which is applied to all tracks passing loose requirements, and which takes positional (e.g., impact parameter) and kinematic (e.g., p_T) information on a track to determine whether it appears to have come from the decay of a B hadron. The Bness tagger is therefore able to extract information from all but a few percent of B jets, and can achieve a very high efficiency for a reasonable level of purity. This robust property of the tagger makes it useful for analyses where efficiency is critical, as is the case with light Higgs boson analyses or even searches for hadronic decays of heavy gauge bosons (see Ref. [10] for more details). A track-by-track NN very similar to that employed by the Bness tagger is used to evaluate tracks in HOBIT; this will be described in Section 5. One drawback of the Bness tagger is that, like SecVtx and unlike RomaNN, it is only able to fit one vertex per jet. Additionally, it uses fewer vertex-based inputs than the RomaNN tagger, and therefore only its track-by-track algorithm is used in HOBIT.

4. The CDF Detector

The CDF II detector is described in detail elsewhere [11]. The detector is cylindrically symmetric around the proton beam line[2] with tracking systems that sit within a superconducting solenoid which produces a 1.4 T magnetic field aligned coaxially with the $p\bar{p}$ beams. A set of calorimeters and muon detectors, to be described later, surround the tracking systems and solenoid.

The outermost tracking system, the Central Outer Tracker (COT), is a 3.1 m long open cell drift chamber which performs up to 96 track position measurements in the region between 0.40 and 1.37 m from the beam axis,

[2]The proton beam direction is defined as the positive z direction. The rectangular coordinates x and y point radially outward and vertically upward from the Tevatron ring, respectively. Transverse energy, and transverse momentum are defined as $E_T{=}E\sin\theta$, and $p_T{=}p\sin\theta$, respectively, θ having been defined in Sec. 3

providing coverage in the pseudorapidity region $|\eta| \leq 1.0$ [12] . Sense wires are arranged in eight alternating axial and $\pm 2^\circ$ stereo "superlayers" with 12 wires each. The position resolution of a single drift time measurement is about 140 μm.

Charged-particle trajectories are found first as a series of approximate line segments in the individual axial superlayers. Two complementary algorithms associate segments lying on a common circle, and the results are merged to form a final set of axial tracks. Track segments in stereo superlayers are associated with the axial track segments to reconstruct tracks in three dimensions.

A five layer double-sided silicon microstrip detector (SVX) covers the region between 2.5 to 11 cm from the beam axis. Three separate SVX barrel modules along the beam line together cover a length of 96 cm, approximately 90% of the luminous beam interaction region. Three of the five layers combine an r-ϕ measurement on one side and a 90° stereo measurement on the other, and the remaining two layers combine an r-ϕ measurement with small angle stereo at $\pm 1.2^\circ$. The typical silicon hit resolution is 11 μm. Additional Intermediate Silicon Layers (ISL) at radii between 19 and 30 cm from the beam line in the central region link tracks in the COT to hits in the SVX.

Silicon hit information is added to COT tracks using a progressive "outside-in" tracking algorithm in which COT tracks are extrapolated into the silicon detector, associated silicon hits are found, and the track is refit with the added information of the silicon measurements. The initial track parameters provide a width for a search road in a given layer. Then, for each candidate hit in that layer, the track is refit and used to define the search road into the next layer. This stepwise addition of precision SVX information at each layer progressively reduces the size of the search road, while also accounting for the additional uncertainty due to multiple scattering in each layer. The search uses all candidate hits in each layer to generate a small tree of final track candidates, from which the tracks with the best χ^2 are selected. The efficiency for associating at least three silicon hits with an isolated COT track is $91 \pm 1\%$. The extrapolated impact parameter resolution for high-momentum outside-in tracks is much smaller than for COT-only tracks: 40 μm, dominated by a 30 μm uncertainty in the beam position.

Outside the tracking systems and the solenoid, segmented calorimeters with projective geometry are used to reconstruct electromagnetic (EM) showers and jets. The EM and hadronic calorimeters are lead-scintillator and iron-scintillator sampling devices, respectively. The central and plug calorimeters are segmented into towers, each covering a small range of pseudorapidity and azimuth, and in full cover the entire 2π in azimuth and the pseudorapidity regions of $|\eta|<1.1$ and $1.1<|\eta|<3.6$ respectively. The transverse energy, E_T, where the polar angle is calculated using the measured z position of the event vertex, is measured in each calorimeter tower. Proportional chambers and scintillation detectors arranged in strips measure the transverse profile of EM showers at a depth corresponding to the shower maximum.

High-momentum jets, photons, and electrons leave isolated energy deposits in contiguous groups of calorimeter towers which can be summed together into an energy "cluster". Electrons are identified in the central EM calorimeter as isolated, mostly electromagnetic clusters that also match with a track in the pseudorapidity range $|\eta| < 1.1$. The electron transverse energy is reconstructed from the measured energy in the electromagnetic cluster with precision $\sigma(E_T)/E_T = 13.5\%/\sqrt{E_T(\mathrm{GeV})} \oplus 2\%$, where the $\oplus$ symbol denotes addition in quadrature. Jets are identified as a group of electromagnetic and hadronic calorimeter clusters using the JETCLU algorithm [13] with a cone size of $\Delta R = 0.4$. Jet energies are corrected for calorimeter nonlinearity, losses in the gaps betwen towers, multiple primary interactions, the underlying event, and out-of-cone losses [14] . The jet energy resolution is approximately $\sigma_{E_T} = 1.0\ \mathrm{GeV} + 0.1 \times E_T$.

Directly outside of the calorimeter, four-layer stacks of planar drift chambers detect muons with $p_T > 1.4$ GeV/c that traverse the five absorption lengths of the calorimeter. Farther out, behind an additional 60 cm of steel, four layers of drift chambers detect muons with $p_T > 2.0$ GeV/c. The two systems both cover the region $|\eta| \leq 0.6$, though they have different structures, and therefore places where the geometrical coverage does not overlap. Muons in the region $0.6 \leq |\eta| \leq 1.0$ pass through at least four drift layers arranged in a conic section outside of the central calorimeter. Muons are identified as isolated tracks in the COT that extrapolate to track segments in one of the four-layer stacks.

5. The HOBIT Tagger

The HOBIT tagger is similar to other multivariate b-tagging algorithms previously used at CDF, such as the RomaNN and Bness taggers. All of these taggers attempt to make maximal use of the available information in b jets, and construct a continuous discriminating variable. HOBIT improves upon these earlier taggers, however, by addressing specific weaknesses of each and optimizing for light Higgs boson searches.

5.1. The architecture

HOBIT is constructed as a feed-forward multilayer perceptron neural network implemented using the TMVA package for Root [15]. It consists of two hidden layers of 25 and 26 nodes, there being 25 inputs to the tagger, and a hyperbolic tangent activation function. Five hundred cycles were used in the training. The training regimen used b jets in Pythia [9] 120 GeV/c^2 Higgs boson Monte Carlo (MC) and light jets from Alpgen-generated Pythia W+jets MC. Charm jets were not considered during training due to preliminary studies which indicated a relative insensitivity of light Higgs boson searches to charm jet contamination. Here, "b jet" denotes a jet with a B hadron within a cone of $\Delta R < 0.4$ of the jet axis, while a "charm jet" contains a charm hadron but no B hadrons within this cone and a "light jet" contains neither B hadrons nor charm hadrons within this cone. Jets were required to have an $E_T > 15$ GeV, $|\eta| < 2$, and at least one track for use in the track-by-track NN described in Sec. 5.3.

The 25 inputs to the tagger are a combination of RomaNN and Bness inputs, albeit with some exceptions, additions and modifications. Fourteen of these inputs are also inputs to the RomaNN tagger. A further ten inputs to HOBIT are the ten highest track-by-track NN discriminant output values of tracks in the jet cone. In the event that there are fewer than ten tracks in a jet, the value of the remaining track-by-track NN inputs are set to -1 as this is the light-jet-like value of the NN output. The number of tracks which pass the track-by-track NN selection criteria is found to have additional discriminating power and is also used as an input to HOBIT. Track selections differ between tracks used for RomaNN inputs and tracks evaluated with the track-by-track NN. Tracks used for RomaNN inputs must have $p_T > 1$ GeV/c and be within $\Delta R < 0.4$ of the jet axis (the same selection used in the published RomaNN tagger), while tracks used by the track-by-track NN inputs had a looser requirement of $p_T > 0.5$ GeV/c and a distance of $\Delta R < 0.7$ from the jet axis (the original requirement was $\Delta R < 0.4$). Other selection cuts were considered, but none resulted in an improvement in the performance of HOBIT. Note that one of the RomaNN inputs used (also used in the Bness tagger) is the E_T of the jet itself. The various HOBIT inputs are correlated with E_T, so the E_T provides additional useful information to

HOBIT. We prevent kinematic biasing of HOBIT by weighting the light jet training sample to have the same E_T distribution as the b-jet training sample.

As previously mentioned, one potential weakness of the RomaNN tagger is its inability to produce a useable output when there is insufficient input information. This requirement of "RomaNN taggability" can be a liability when very high b-jet tagging efficiency is sought. In the MC sample used to train the HOBIT tagger, 21% of b jets fail to be RomaNN taggable, versus 30% of light jets. The track-by-track NN in HOBIT compensates for this shortfall of RomaNN. While jets in HOBIT are required to have at least one track with an evaluated track-by-track NN output, only 3.0% of b jets and 2.1% of light jets in the MC fail this requirement, indicating a very efficient taggability requirement.

The full list of inputs to HOBIT ranked by importance after TMVA's training is provided in Table 1. Here, "importance" refers to the sum of the squares of the weights connecting a given input to the nodes of the first hidden layer of HOBIT. Distributions of the inputs to HOBIT are shown in Fig. 1. A description of these inputs is given below.

5.2. The RomaNN inputs

RomaNN inputs used in HOBIT consist of observables built using tracks and vertices found to be "heavy-flavor-like" (HF-like) according to its NNs. No modifications were made to the RomaNN inputs compared to the published tagger. These inputs include:

- The invariant mass, pseudo-$c\tau$, 3-d displacement and 3-d displacement significance of the most HF-like vertex.
- The number of tracks both in HF-like vertices and standalone HF-like tracks associated to a displaced vertex, as well as their combined invariant mass, and the ratio of the scalar sum of the p_T's of these tracks to the scalar sum of the p_T's of all tracks in the jet.
- The loose SecVtx tag status, as well as the mass of the tracks used in the loose SecVtx vertex fit.

5.3. Bness inputs: the track-by-track NN

As mentioned above, the ten highest evaluated track-by-track NN outputs for tracks in a jet serve as inputs to HOBIT. Therefore, this section concerns the track-by-track NN itself. The input variables to the track-by-track NN are the same for HOBIT as were used in the track-by-track NN of the original Bness tagger. However, the track-by-track Bness NN was retrained to create the HOBIT track-by-track NN. This was done not only because the cone requirement on the tracks was loosened but also because we wished to optimize the track-by-track NN for light Higgs boson searches. Hence, while the original Bness track-by-track NN was trained using $ZZ \rightarrow 4$ jets MC, the HOBIT track-by-track NN was trained using the same MC as was used to train the overall HOBIT tagger. Since the track-by-track NN operates at the level of individual tracks, we impose an additional requirement on b-jet tracks for the purposes of training by demanding that they be within $\Delta R < 0.05$ of the actual charged particles resulting from a B hadron decay in the MC. The track-by-track NN employed the same basic framework for training as that used for HOBIT itself (training cycles, inner layer structure, etc.).

Some of the inputs to the track-by-track NN take advantage of the fact that tracks from B hadron decays are displaced from the primary vertex. These inputs include the impact parameter, the distance along the z-axis between the track and the primary vertex, and the significance of each. Kinematic inputs such as the p_T, rapidity, and track momentum perpendicular to the jet axis (p_{perp}) exploit the greater collimation of B tracks due to the large boost of the hadron. Finally, the jet E_T is an input to the track-by-track NN, because the previously mentioned inputs are correlated with jet E_T. Tracks from light jets are weighted in training such that the jets which contain them have the same E_T distribution as the b jets; this is done so as to avoid kinematic biasing in the track-by-track NN. Distributions of the track-by-track NN inputs are shown in Fig. 2. Not shown are the jet E_T distributions, which are identical by construction.

5.4. HOBIT Performance

The output HOBIT distributions for b-jets and light-jets from an independent but identically generated MC sample as was used to train the discriminator are shown in Fig. 3. In Fig. 4, the b-jet efficiencies and the light jet efficiencies ("mistag rates") as a function of jet E_T and η are shown for two HOBIT operating points – a requirement of a HOBIT output > 0.72 ("loose") and a requirement of a HOBIT output > 0.98 ("tight"). At higher η, where tracking coverage is more sparse and less information is available, the b-tagging efficiency drops, as would be expected. Interestingly, the mistag rate increases in the case of the loose tag and drops in the case of the tight

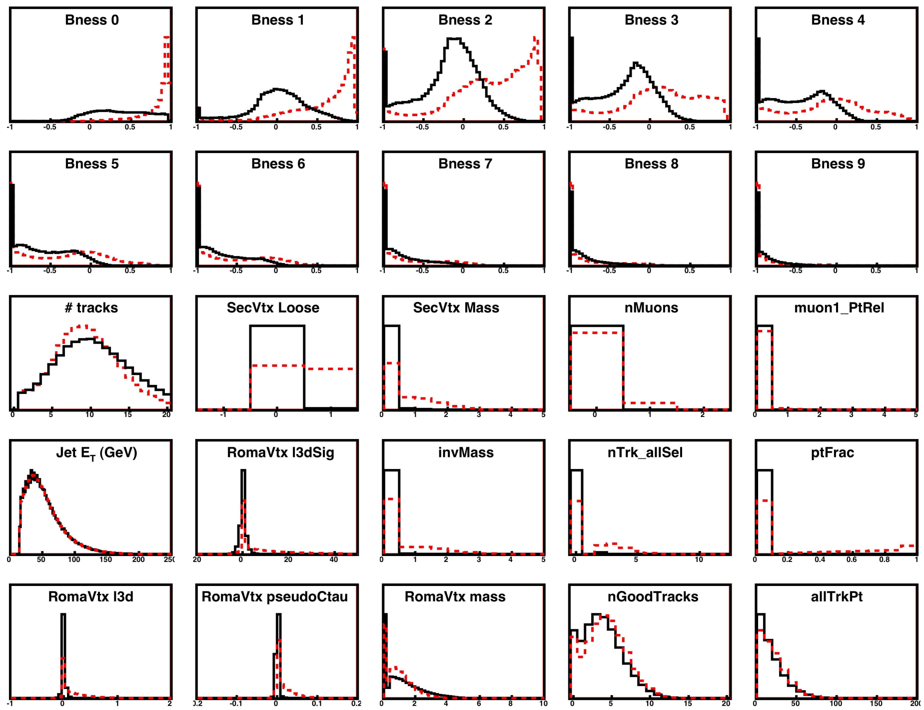

Figure 1: Inputs to HOBIT. The solid histogram is for light quark jets and the dashed (colored) histogram is for b jets. Taken from MC, the distributions are normalized to one another. Left to right, top to bottom: the Bness value for the 10 highest Bness tracks; the number of Bness-selected tracks; the loose SecVtx tag status and the mass of its fitted vertex; the number of SLT-tagged muons and the momentum transverse to the jet axis of the most SLT-favored muon; jet E_T; the 3-d displacement significance of the most HF-like vertex in RomaNN; the invariant mass, number, and fraction of total track p_T of HF-like tracks; the 3-d displacement, pseudo-$c\tau$ and invariant mass of the most HF-like vertex; the number of RomaNN-selected tracks and their total p_T.

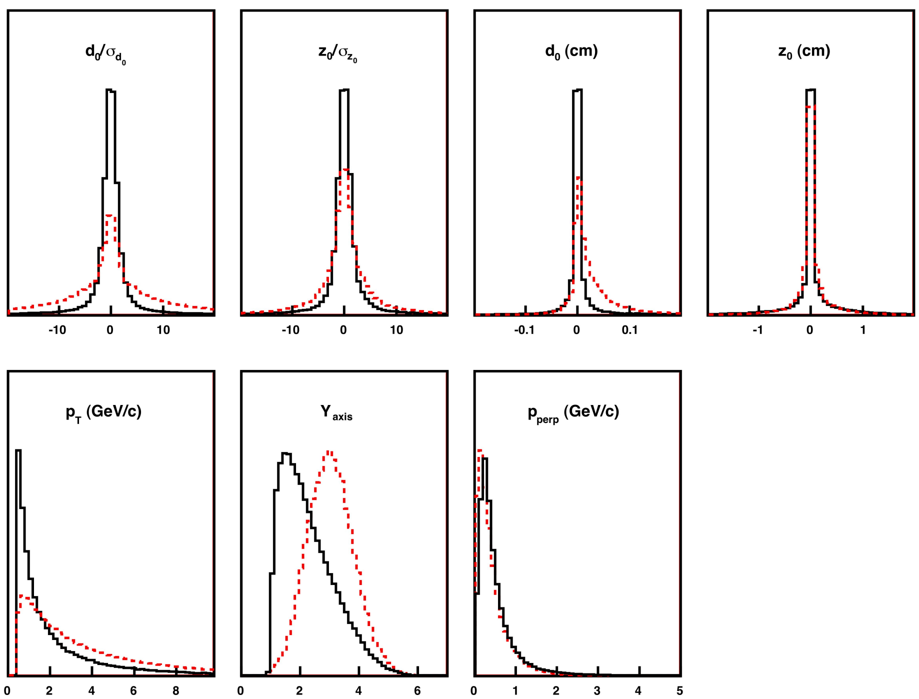

Figure 2: Inputs to track-by-track NN. The solid histogram is for tracks in light quark jets and the dashed (colored) histogram is for tracks in b jets; taken from MC, the distributions are normalized to one another. Not shown is the jet E_T, identical between the two distributions by construction. Left-to-right, top-to-bottom: significance of the impact parameter and Δz between the track and the primary vertex; the values of the impact parameter and Δz; the p_T of the track with respect to the beam axis; and the track's rapidity and p_T with respect to the jet axis.

tag, demonstrating the higher impact of incorrectly identified tracks when using a loose tagging requirement. In general, the efficiency increases with increasing jet E_T due to the greater displacement of the B hadron. Similarly, the light jet efficiency increases, at least in part due to the higher rapidity and p_T of tracks in high-E_T jets.

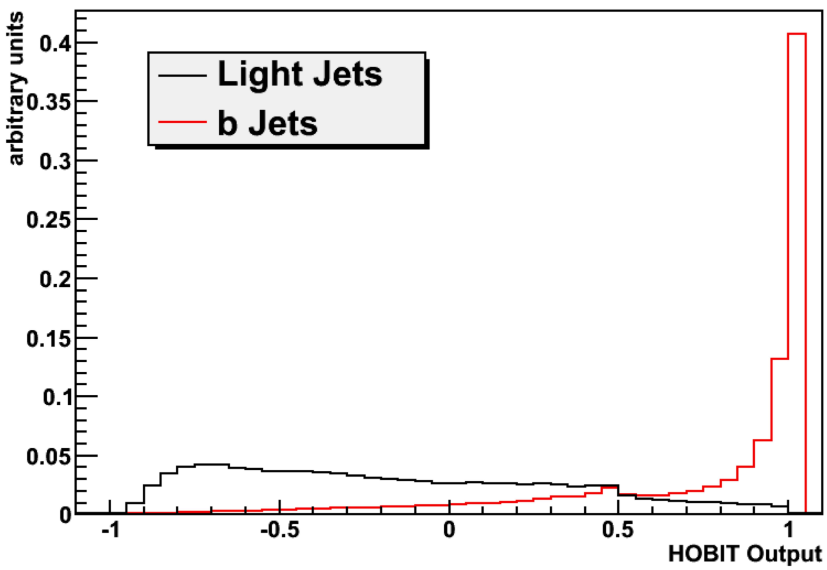

Figure 3: HOBIT outputs. The output is trained so that 1 is b jet-like and -1 is targeted to be light jet-like. The black histogram is for light quark jets and the colored histogram is for b jets. Taken from MC, the distributions are normalized to one another.

The performance of a tagger is best evaluated by comparing its purity to tagging efficiency at given operating points. We compare HOBIT's purity versus efficiency curve to the curves of the Bness and RomaNN taggers and to the purity versus efficiency performance of SecVtx at both its tight and loose operating points (Fig. 5). Here, purity refers to the fraction of light-jets in W+jets MC which are not tagged as b-jets, and efficiency refers to the fraction of b jets in light Higgs boson MC which are tagged. When evaluating tag efficiencies, the jets in both the numerator and denominator are required to have $E_T > 15$ GeV and $|\eta| < 2$, the same E_T and η requirements as were placed on the jets in the training of HOBIT. Fig. 5 shows that for a given purity level, improvement in the absolute efficiency due to HOBIT is

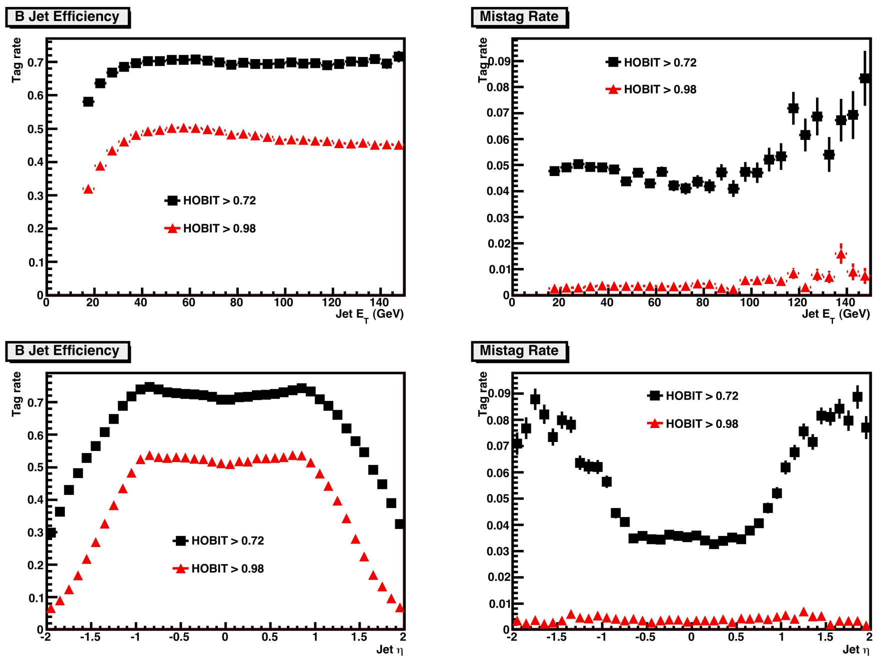

Figure 4: The b-jet and light-jet efficiencies in MC before SF corrections as a function of η and E_T. The black triangles are for the looser operating point and the colored triangles are for the tighter operating point.

approximately 10% over the Bness and RomaNN taggers, and approximately 15% over the SecVtx tagger.

We investigated how much of the improvement in HOBIT over earlier taggers is due to the optimization on jets that specifically originated from Higgs boson decays. To study this, we trained NN taggers that take the same inputs as Bness and RomaNN using W+jets and light Higgs boson MC, then compared the purity versus efficiency curve with those of the original Bness and RomaNN taggers, which were trained using ZZ MC and Z+jets MC, respectively. The results can be seen in Figs. 6 and 7. In the case of the RomaNN comparison, not only is our retrained RomaNN tagger compared with the original RomaNN result, but also with RomaNN's b versus light jet separator. This is because the architecture of RomaNN consisted of three different NN separators (b versus light, b versus charm, light versus charm) which fed into the final RomaNN separator. As we retrained using light and b jets, the comparison of the Higgs-optimized version of the RomaNN tagger with the original b versus light separator makes for a more fair comparison. In both the Bness and RomaNN cases, the improvement in absolute efficiency is approximately 2%.

6. Efficiency and Mistag Scale Factors

In order to be used in a physics analysis, the performance of the HOBIT b tagger must be calibrated. Historically, MC modeling of b-tag efficiencies and mistag rates has not been sufficient to use the uncorrected predictions of the MC. Instead, we use various techniques to measure the b-tagging efficiency and the mistag rate using CDF data. Examples of such techniques applied to the SecVtx algorithm are using jets containing electrons (therefore HF-enriched) for measuring the b-tagging efficiency [16], and using the rate at which jets have a displaced vertex reconstructed behind the primary vertex ("negative tags") to estimate mistags [17]. For the tight SecVtx tagger, the b-tag efficiency is found to be well predicted by the MC up to a scale factor (SF), where SF $= 0.96 \pm 0.05$ for the full CDF dataset. In order to utilize HOBIT to predict yields in data from MC simulation, a similar level of uncertainty in HOBIT's SF to that of SecVtx's SF is needed for each operating point.

An important difference between SecVtx and HOBIT is the absence of negative tags in HOBIT, meaning the SecVtx mistag calculation technique cannot be applied. Instead, we use two new techniques described below

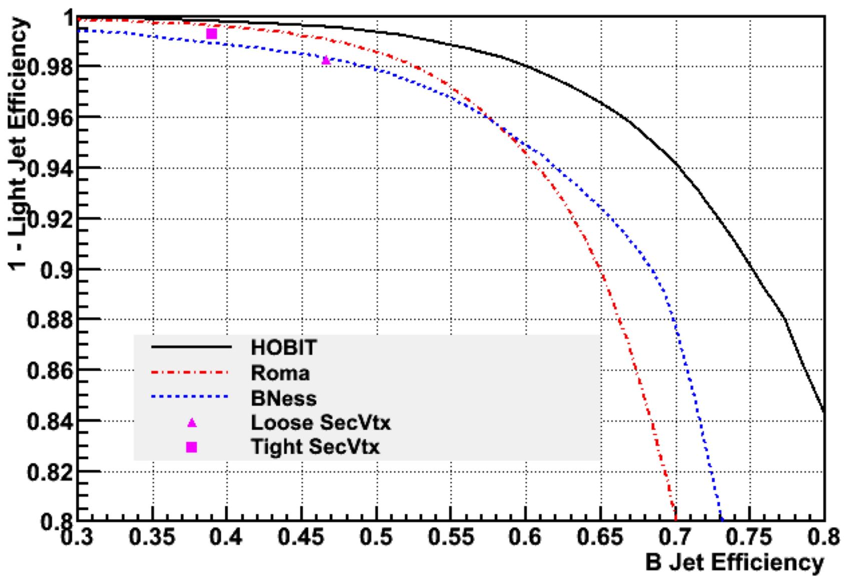

Figure 5: A comparison of the purity-efficiency tradeoffs for HOBIT versus RomaNN, Bness, and SecVtx loose and tight. A significant improvement over prior multivariate taggers is seen.

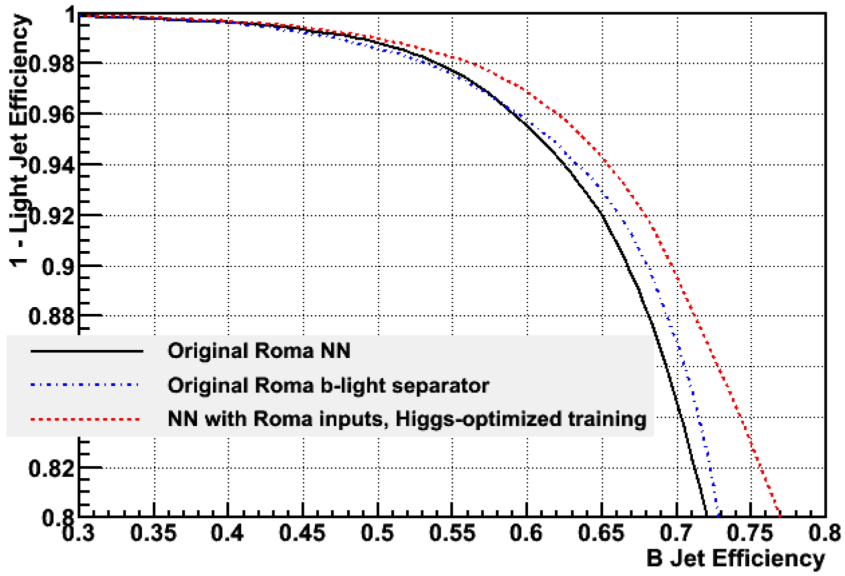

Figure 6: A comparison of the purity-efficiency tradeoffs for the original RomaNN tagger (as well as its b-light separator) and our version of the Higgs-optimized RomaNN tagger.

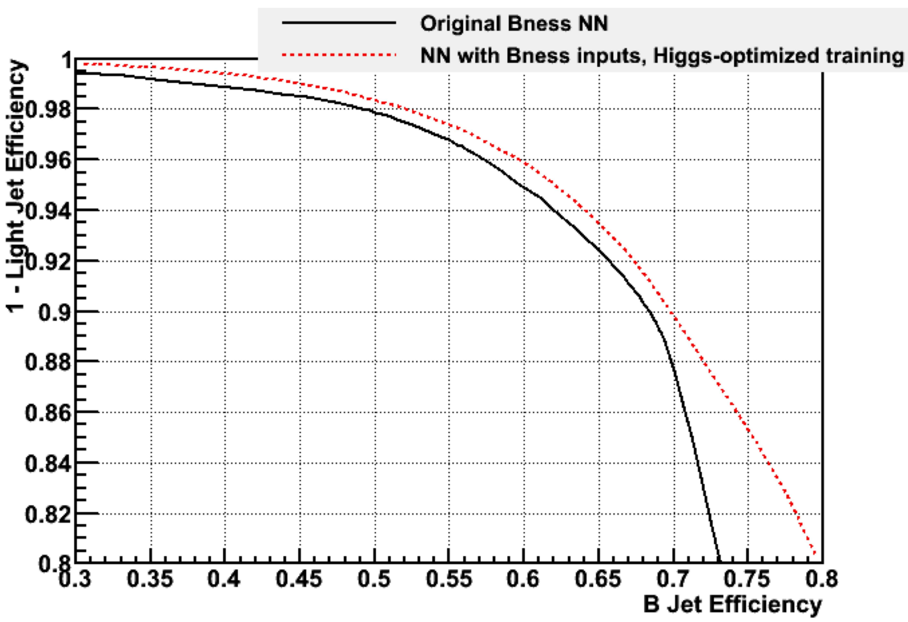

Figure 7: A comparison of the purity-efficiency tradeoffs for the original Bness tagger and our version of the Higgs-optimized Bness tagger.

for calibrating b-tag SFs and providing mistag rates: the "$t\bar{t}$ cross section method", and the "electron conversion method".

6.1. Scale factors using the $t\bar{t}$ cross section method

The $t\bar{t}$ cross section method seeks to calibrate the predicted b-tagging efficiency and the mistag rate in MC to match those measured in data using $t\bar{t}$ candidate events in a W+3-or-more-jets sample under the assumption that the $t\bar{t}$ cross section is known. The method is based upon a previous analysis [18] that simultaneously measured the SecVtx b-tag SFs and the $t\bar{t}$ cross section. In that measurement, the rates of singly and double tagged events provide a constraint which allows the measurement of two unknowns. A two-dimensional fit was performed to maximize the likelihood of observing the data counts as functions of the SecVtx b-tag SF and the $t\bar{t}$ cross section.

This method has been repurposed such that the $t\bar{t}$ cross section is now an input assumption, allowing for the calibration of the HOBIT b-tag efficiency and the HOBIT mistag rate. We parameterize the resulting tag rate in the MC samples as a 5-dimensional matrix, where each element is the measured rate within a bin of the following five variables: jet E_T, jet η, the number of tracks in the jet, the number of primary vertices in the event, and the z location of the primary vertex from which the jet is calculated to have originated. The matrix is similar to the SecVtx mistag matrix [17], although of a lower dimension; the variables it has in common with the SecVtx mistag matrix have the same binning between the two matrices. For eight different HOBIT operating points, separate matrices are constructed for b, charm, and light jets.

The W+3-or-more-jets sample has an insufficient number of mistags to calibrate the mistag SF, so we add a W+1 jet sample, which before b-tagging requirements is almost pure W+light flavor (LF) events. After b tagging, the W+1 jet sample consists of comparably sized $Wb\bar{b}$, $Wc\bar{c}$, Wcj, and mistagged W+LF events. The background predictions [4] involve scaling the total W+jets rate to data and subtracting off the non-W+jets components. The prediction of the W+HF component of W+jets relies on the HF K-factor. This scaling adjusts leading-order theoretical predictions of the fraction of HF in W+jets events to account for higher-order corrections. We find that the $W+1$-jet data provides an independent handle on the mistag SF while the b-tag SF is constrained by the events with three or more jets. However, the dependence on the HF K-factor introduces a systematic uncertainty that strongly affects the mistag SF. For low values of the HOBIT cut, the mistag rate is relatively high, and the relative contribution to the tagged W+1-jet sample from W+HF events is lower. This translates to a systematic uncertainty on the mistag SF due to the uncertainty on the HF K-factor that is lower at low HOBIT output values than at high HOBIT output values.

The maximum of the 2-d likelihood for the b-tag SF and the mistag SF is calculated given the observed data and fixed values of the HF K-factor, the $t\bar{t}$ cross section, and the minimum HOBIT output value. The dependence on the HF K-factor and the $t\bar{t}$ cross section are then taken as sources of systematic uncertainty. We assume $\sigma_{t\bar{t}} = 7.04 \pm 0.704$ pb [19], and take the HF K-factor to be 1.4 ± 0.4.

The fitted b-tag and mistag SFs are shown in Figures 8 and 9, respectively, as functions of the minimum HOBIT output value. The curves represent a linear fit to the b-tag SF as a function of the minimum HOBIT output value, and a parabolic fit to the mistag SF. The variation due to $\sigma_{t\bar{t}}$ is also shown, where we take the larger of the two shifts in the result due to an increase/decrease in $\sigma_{t\bar{t}}$ and then symmetrize the uncertainty.

The determination of the b-tag and mistag SFs are subject to the same sources of systematic uncertainty as a measurement of $\sigma_{t\bar{t}}$ [20]. Specifically, the $t\bar{t}$ acceptance depends on initial-state radiation and final-state radiation (ISR+FSR), parton distribution functions (PDFs), jet energy scale, trigger efficiencies and lepton identification efficiencies. The luminosity uncertainty, although nearly absent in the results of Ref. [20], also contributes to the overall systematic uncertainty.

For the loose (0.72) and tight (0.98) HOBIT operating points, this method yields efficiency SFs of 0.997 ± 0.037 and 0.917 ± 0.069, respectively. The mistag rate SFs are 1.391 ± 0.202 and 1.515 ± 0.291. A complete table of systematic uncertainties for the efficiency SF is shown in Table 2, and for the mistag matrix SF in Table 3. Figures 10, 11, 12, 13, and 14 show validation plots comparing properties of the highest E_T jet (HOBIT output, and select HOBIT inputs) in $WH \rightarrow l\nu b\bar{b}$ candidate events before any b-tag requirements or SF corrections are applied for MC versus data. Good agreement is seen between MC and data.

6.2. Scale factors using the electron conversion method

A second method of calculating the correction for the HOBIT MC response involves a modification of the traditional SecVtx efficiency SF algorithm in a way that does not require the concept of a "negative tag" [16].

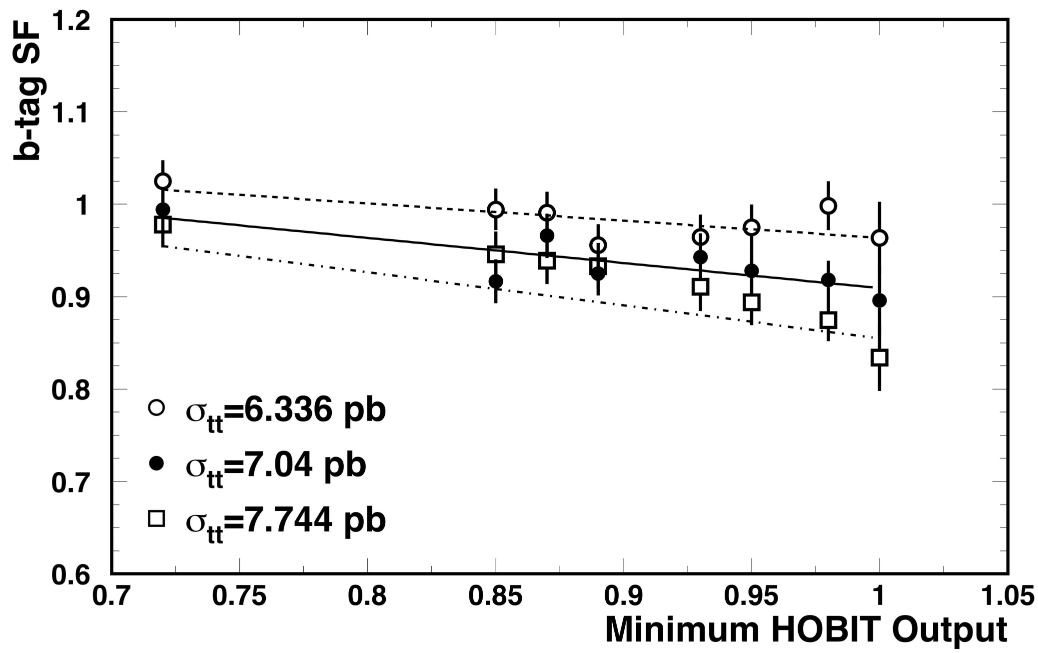

Figure 8: The measured value of the b-tag scale factor for the HOBIT tagger as a function of the minimum HOBIT output value. Variations are shown assuming two values of the $t\bar{t}$ cross section.The straight lines are fits to the SFs assuming the central value of the $t\bar{t}$ cross section, and $\sigma_{t\bar{t}} = 6.336$ pb, the more conservative case for the purpose of estimating uncertainties. The latter fit has been reflected through the central line to obtain a symmetric uncertainty band.

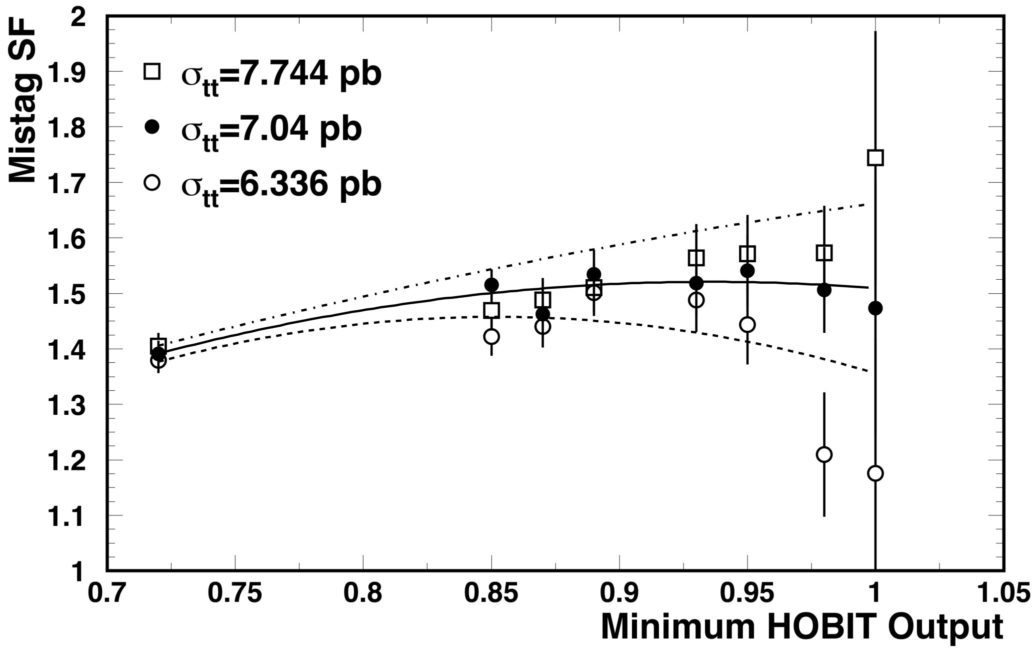

Figure 9: The measured value of the mistag scale factor for the HOBIT tagger as a function of the minimum HOBIT output value. Variations are shown assuming two values of the $t\bar{t}$ cross section. Parabolas are fit to the results assuming the central value of the $t\bar{t}$ cross section, and for $\sigma_{t\bar{t}} = 6.336$ pb. The latter has been reflected through the curve for the central value to obtain the depicted uncertainty band.

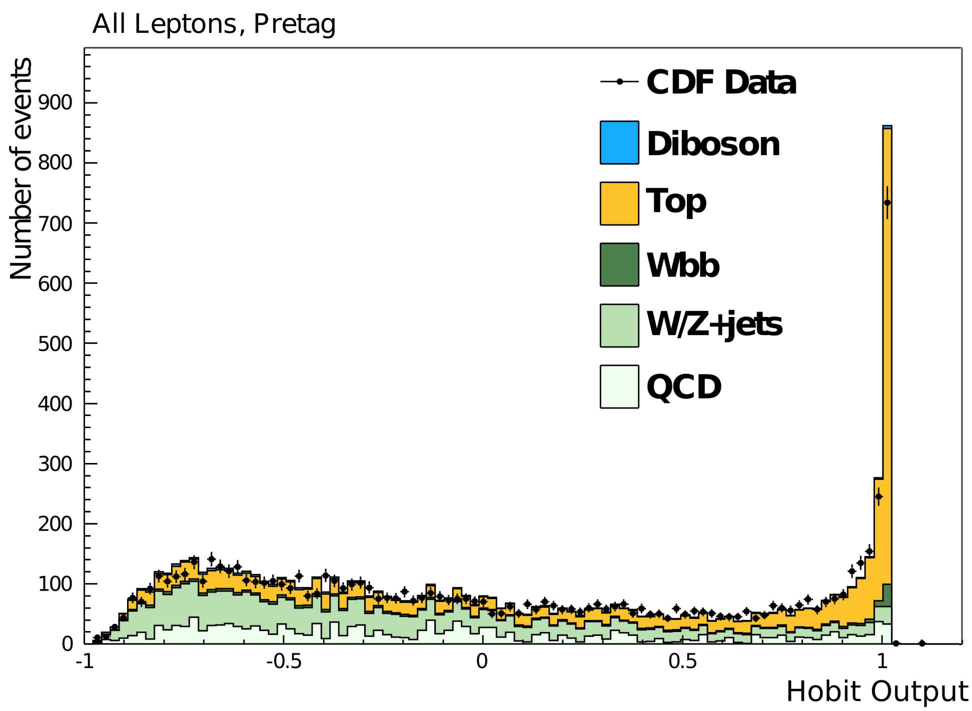

Figure 10: Data versus MC, the HOBIT output distribution of the highest E_T jet from events in the $WH \to l\nu b\bar{b}$ sample before a requirement of a b-jet tag.

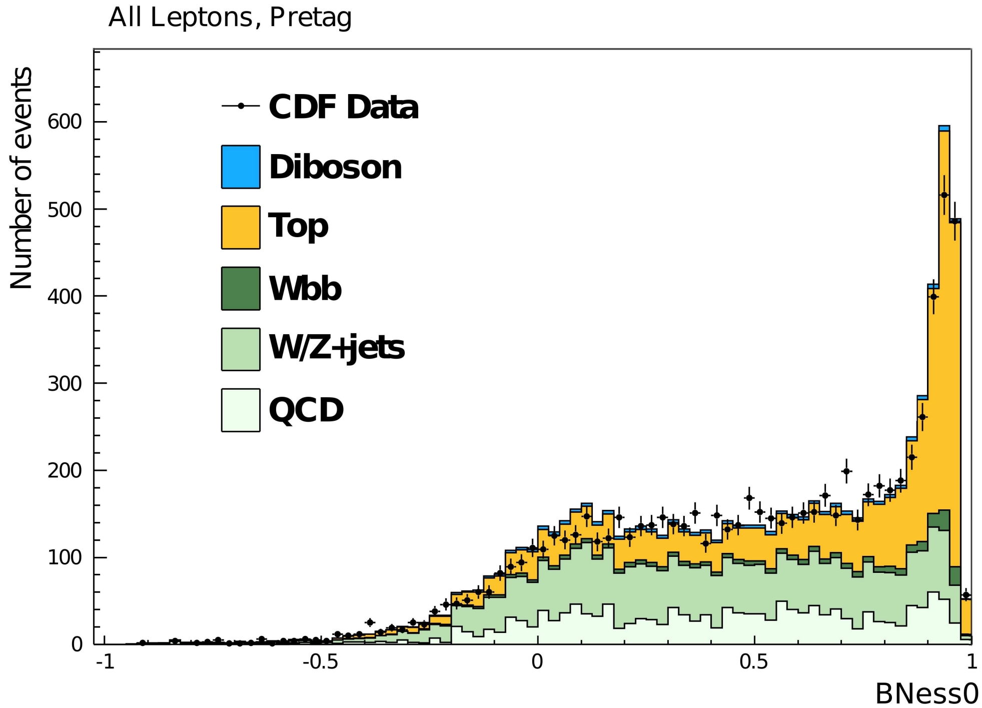

Figure 11: Data versus MC, highest track Bness of the highest E_T jet from events in the $WH \to l\nu b\bar{b}$ sample before a requirement of a b-jet tag.

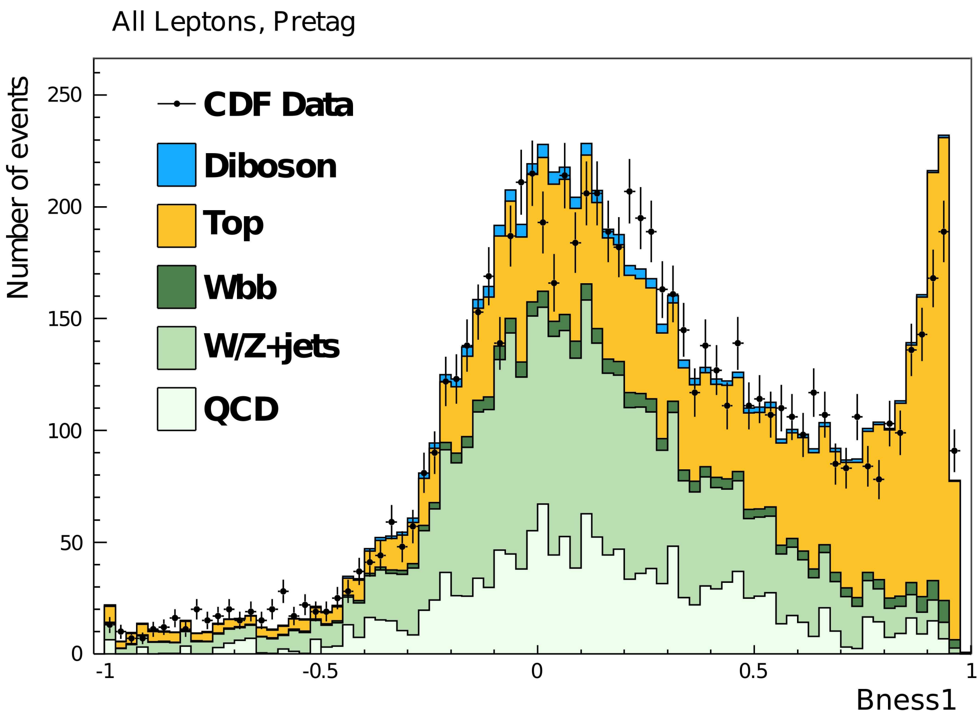

Figure 12: Data versus MC, second highest track Bness of the highest E_T jet from events in the $WH \to l\nu b\bar{b}$ sample before a requirement of a b-jet tag.

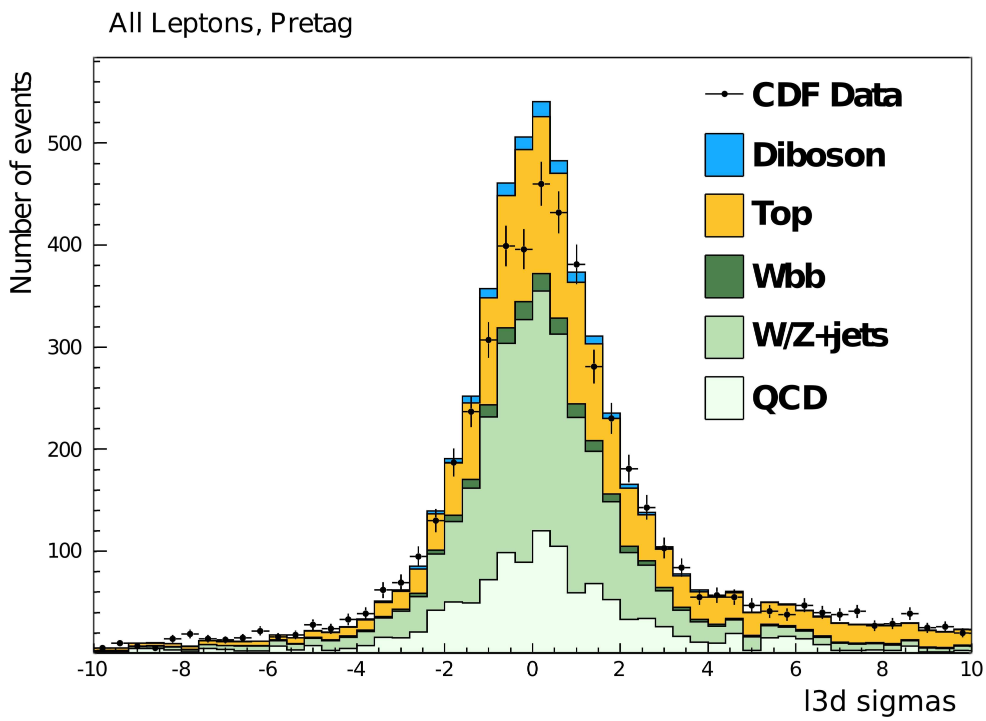

Figure 13: Data versus MC, 3-d displacement significance of most HF-like displaced vertex of the highest E_T jet from events in the $WH \to l\nu b\bar{b}$ sample before a requirement of a b-jet tag.

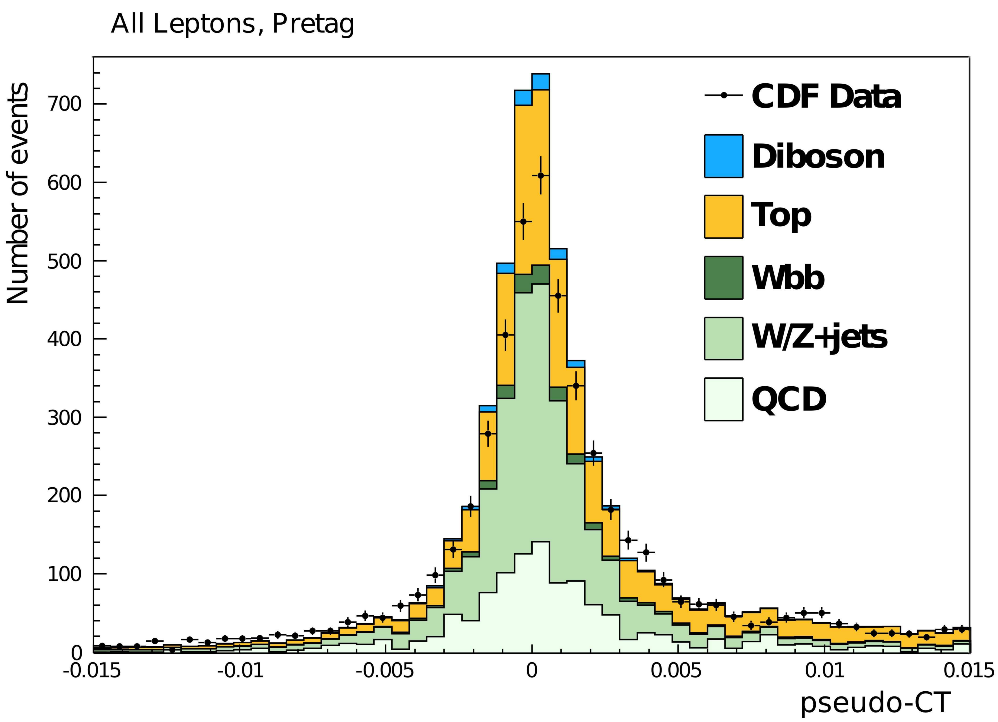

Figure 14: Data versus MC, pseudo-cτ of most HF-like displaced vertex of the highest E_T jet from events in the $WH \rightarrow l\nu b\bar{b}$ sample before a requirement of a b-jet tag.

However, like the SecVtx technique, this method takes advantage of the HF enhancement among jets containing electrons, discriminating between HF and LF jets based upon whether the electron is identified as coming from a photon conversion.

The event sample consists of back-to-back dijet events where one jet contains an electron candidate (the electron jet, or "e-jet"), while its opposite jet has no such requirement (the away jet, or "a-jet"). We can label each jet originating either from an HF quark ("B") or a light flavor quark or gluon ("Q") and categorize each event as N_{XY}, where the e-jet has flavor X and the a-jet has flavor Y. Then the total number of events (N^e) is

$$N^e = N_{BB} + N_{BQ} + N_{QB} + N_{QQ}$$

and the HF fraction of the e-jets is

$$F_B = (N_{BB} + N_{BQ})/N^e.$$

Applying a b tag on the e-jet with a tagging efficiency (ϵ^e) and a mistag rate (ϵ_{mis}), the number of b-tagged e-jets (N^e_+) is

$$N^e_+ = \epsilon^e \cdot (N_{BB} + N_{BQ}) + \epsilon^e_{mis} \cdot (N_{QB} + N_{QQ}).$$

Assuming the fraction of light flavor jets with conversions is f^c and the conversion finding efficiency is ϵ^c for the light flavor jets and ϵ^0 for the HF jets, we can obtain the number of e-jets identified from the conversion N^{ec} as

$$N^{ec} = \epsilon^0 \cdot (N_{BB} + N_{BQ}) + \epsilon^c \cdot f^c \cdot (N_{QB} + N_{QQ})$$

After tagging, the number of b-tagged conversion e-jets (N^{ec}_+) becomes

$$N^{ec}_+ = k \cdot \epsilon^e \cdot \epsilon^0 \cdot (N_{BB} + N_{BQ}) + \epsilon^e_{mis} \cdot \epsilon^c \cdot f^c \cdot (N_{QB} + N_{QQ}),$$

where k is the ratio of the b-tag efficiency for an HF e-jet identified as a conversion to that for one that is not.

The previous two equations allow us to solve for ϵ_{mis} and ϵ^e:

$$\epsilon_{mis} = (N^{ec}_+ - k \cdot \epsilon^0 \cdot N^e_+)/(N^{ec} - \epsilon^0 \cdot N^e \cdot (k + (1-k) \cdot F_B))$$

and

$$\epsilon^e = (N^e_+ - \epsilon_{mis} \cdot N^e \cdot (1 - F_B))/(N^e \cdot F_B).$$

Here, all terms that are not the mistag and efficiency rates can be counted directly in data, taken from MC (k), measured in data (F_B) or both taken from MC and/or measured in data (ϵ^0). In the case of F_B, we can simply use the traditional SecVtx electron method [16] to give us this value. For ϵ^0, obtaining this quantity from MC is trivial, as we have truth information available. To calculate it from data, we look at the rate at which positively SecVtx-tagged jets are found to contain conversion electrons and then adjust this rate using negatively-SecVtx-tagged jets.

The resulting tagging efficiency SFs for the loose and tight HOBIT outputs are 0.986 ± 0.066 and 0.949 ± 0.044 respectively, in good agreement with the results from the $t\bar{t}$ method. Some of the largest contributors to the systematic component of these uncertainties includes the difference between the results when we use the MC-calculated ϵ^0 versus the data-calculated version and the fact that b-jets containing electrons tend to leave fewer tracks than typical b-jets.

The SFs on the mistag rate for the loose and tight HOBIT operating points are 1.28 ± 0.17 and 1.42 ± 0.89, respectively, also consistent with the results of the $t\bar{t}$ method. As a check, we compare e-jets in data and MC (Figs. 15 and 16), after purifying the HF content by requiring the away jet to be tight SecVtx tagged and the electron in the e-jet to not be identified as a conversion. The fraction of HF versus light jet MC used in these plots is determined via a fit of MC templates to the HOBIT distribution in data.

6.3. SF Combination

When combining the correction SFs for the MC b-tag efficiency from the electron and $t\bar{t}$ method, we obtain 0.993 ± 0.032 (for HOBIT's loose operating point, 0.72) and 0.937 ± 0.037 (HOBIT's tight operating point, 0.98). The combined results for the mistag rates are 1.331 ± 0.130 and 1.492 ± 0.277, respectively. Due to the uncertainties in the electron and $t\bar{t}$ methods being uncorrelated, the combination is straightforward. This results in a greater than 25% reduction in the size of the uncertainty on the b-tag efficiency in comparison to the previous most widely used CDF b-tagging algorithm, SecVtx.

7. Conclusion

We have developed an NN-based b identification tagger which improves upon the best ideas of previous CDF taggers, has a very generous taggability

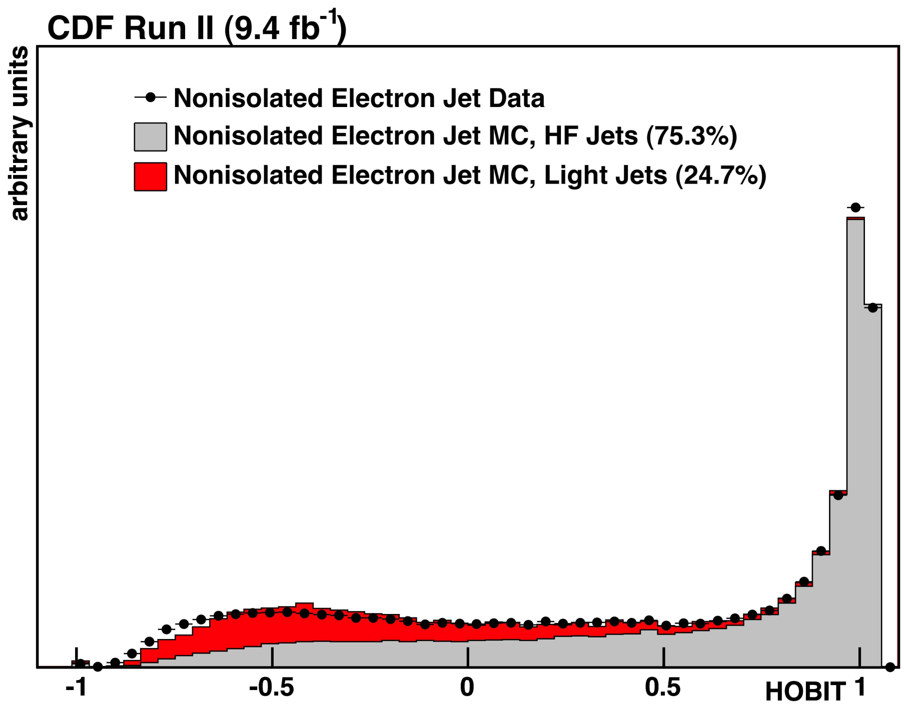

Figure 15: HOBIT output for electron jets, data versus MC. Relative proportions of HF to light jets are determined via a fit of the two MC templates to the data.

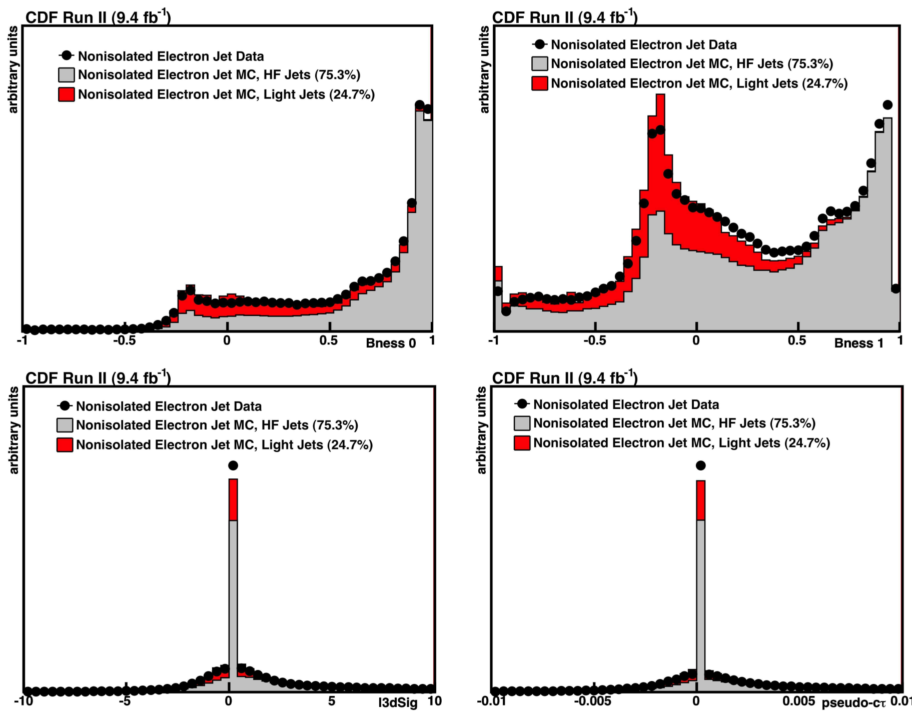

Figure 16: Comparison of select HOBIT inputs for electron jets, data versus MC.

requirement, and has been optimized for $H \rightarrow b\bar{b}$ searches, the primary decay channel of the light Higgs boson at the Tevatron. Using two uncorrelated and innovative methods, we found tagging efficiencies, mistag rates, and data-to-MC scale factors that are in good agreement. The combination of these methods results in a greater than 25% reduction in the b-tag efficiency uncertainty compared to SecVtx, the previous most widely used CDF b-tagging algorithm. In the current light Higgs boson analyses at CDF, we estimate that replacing previous tagging algorithms with HOBIT results in a 10-20% improvement in Higgs boson sensitivity.

Acknowledgements

The authors thank the CDF collaboration, the Fermilab staff and the technical staffs of the participating institutions for their vital contributions. This work was supported by the US Department of Energy and the Fermilab Research Alliance International Fellowship.

[1] V.M. Abazov, et al., b-Jet Identification in the D0 Experiment, Nucl. Instrum. Methods A 620 (2-3) (2010) 490.

[2] CMS Collaboration, Performance of the b-jet Identification in CMS, CMS Physics Analysis Summary.

[3] ATLAS Collaboration, Commissioning of the ATLAS High-Performance b-Tagging Algorithms in the 7 TeV Collision Data, ATLAS CONF Note.

[4] D. Acosta, et al., Measurement of the $t\bar{t}$ Production Cross Section in $p\bar{p}$ Collisions at $\sqrt{s} = 1.96$ TeV Using Lepton+Jets Events with Secondary Vertex b-tagging, Phys. Rev. D 71 (2005) 052003.

[5] D. Acosta, et al., Measurement of the $t\bar{t}$ Production Cross Section in $p\bar{p}$ Collisions at $\sqrt{s} = 1.96$ TeV Using Lepton+Jets Events with Semileptonic B Decays to Muons, Phys. Rev. D 72 (2005) 032002.

[6] C. Ferrazza, Identificazione di quark pesanti in getti adronici in interazioni $p\bar{p}$ con il rivelatore CDF al Tevatron, Master's thesis, Universita "La Sapienza" Roma (2006).

[7] P. Mastrandrea, Study of the heavy flavour fractions in Z+jets events from $p\bar{p}$ collisions at energy = 1.96 TeV with the CDF II detector at the Tevatron collider, FERMILAB-THESIS-2008-63.

[8] J. Freeman, et al., An Artificial Neural Network Based B-Jet Identification Algorithm at the CDF Experiment, Nucl. Instrum. Meth. A, Vol. 663 (2012), pp. 27-37.

[9] T. Sjostrand, S. Mrenna, P. Skands, "PYTHIA 6.4 Physics and Manual", arXiv:hep-ph/0603175v2.

[10] T. Aaltonen, et al., Search for $WZ+ZZ$ Production with Missing Transverse Energy+Jets with b Enhancement at $\sqrt{s}$ =1.96 TeV, Phys. Rev. D 85 (2012) 012002.

[11] A. Abulencia, et al., Measurements of inclusive W and Z cross sections in $p\bar{p}$ collisions at $\sqrt{s} = 1.96$ TeV, J. Phys. G 34 (2007) 2457.

[12] T. Affolder, et al., CDF Central Outer Tracker, Nucl. Instrum. Methods A 526 (3) (2004) 249.

[13] F. Abe, et al., Topology of three-jet events in $p\bar{p}$ collisions at $\sqrt{s} = 1.8$ TeV, Phys. Rev. D 45 (1992) 1448.

[14] A. Bhatti, et al., Determination of the jet energy scale at the Collider Detector at Fermilab, Nucl. Instrum Methods A 566 (2) (2006) 375.

[15] A. Hoecker, P. Speckmayer, J. Stelzer, J. Therhaag, E. von Toerne, and H. Voss, "TMVA: Toolkit for Multivariate Data Analysis," PoS A CAT 040 (2007) [physics/0703039].

[16] Henri Bachacou, A Measurement of the Production Cross Section of $t\bar{t}$ Pairs Using Secondary Vertex b-tagging, FERMILAB-THESIS-2004-48.

[17] D. Acosta, et al., Measurement of the $t\bar{t}$ Production Cross Section in $p\bar{p}$ Collisions at $\sqrt{=}$1.96 TeV Using Lepton+Jets Events with Semileptonic B Decays to Muons, Phys. Rev. D 71, 052003 (2005).

[18] Nazim Hussain, A simultaneous measurement of the b-tagging efficiency scale factor and the $t\bar{t}$ Production Cross Section at the Collider Detector at Fermilab, FERMILAB-MASTERS-2011-02.

[19] U. Langenfeld, S. Moch and P. Uwer, Measuring the running top-quark mass, Phys. Rev. D 80, 054009 (2009).

[20] T. Aaltonen *et al.*, First Measurement of the Ratio $\sigma_{(}t\bar{t})/\sigma_{(}Z/\gamma{*}{*} \rightarrow \ell\ell)$ and Precise Extraction of the $t\bar{t}$ Cross Section, Phys. Rev. Lett. **105**, 012001 (2010).

Jet (HOBIT) Input	Importance
RomaVtx pseudo-cτ	435
RomaVtx 3-d displacement significance	382
Bness 0	77.5
Bness 1	21.5
SecVtx Loose	16.9
Bness 3	9.90
Number of muons	7.80
ptFrac	7.05
Bness 2	6.22
Bness 4	5.46
muon p_T to jet axis	5.32
Bness 5	4.54
Bness 9	4.46
M_{inv} of HF-like tracks	4.17
Bness 6	3.44
Bness 8	2.70
RomaVtx 3-d displacement	2.24
SecVtx Mass	1.68
Bness 7	1.51
RomaVtx Mass	0.752
Number of track-by-track NN tracks	0.380
Number of HF-like tracks	0.287
Jet E_T	0.161
Number of Roma-selected tracks	0.125
Total p_T of tracks	0.00250

Table 1: Inputs to the HOBIT tagger and their importances; ranking is done by importance (see text for definition of this term). "RomaVtx" denotes the most HF-like vertex as found by the RomaNN tagger.

Table 2: The systematic uncertainties for the b-jet tagging efficiency scale factor from the $\sigma(t\bar{t})$ method measurement. This uncertainty must be combined with the electron method scale factor uncertainty; the two should be treated as uncorrelated. The uncertainties shown below are absolute shifts.

b-eff SF $\sigma(t\bar{t})$ method		HOBIT Operating Point	
source		Loose	Tight
$\sigma(t\bar{t})$	up	-0.011	-0.019
	down	0.011	0.019
luminosity	up	-0.004	-0.055
	down	0.007	0.012
jet energy scale	up	-0.005	-0.007
	down	0.005	0.007
generator	up	0.003	0.005
	down	-0.003	-0.005
ISR/FSR	up	-0.001	-0.001
	down	0.001	0.001
$t \rightarrow Wb$ branching ratio	up	-0.001	-0.001
	down	0.001	0.001
Trigger	up	-0.001	-0.001
	down	0.001	0.001
PDF	up	0.001	0.001
	down	-0.001	-0.001
W+j kfactor	up	0.009	0.006
	down	-0.009	-0.006
Statistics	up	0.014	0.008
	down	-0.014	-0.008
total	up	0.022	0.026
	down	-0.022	-0.026

Table 3: The systematic uncertainties for the mistag rate scale factor from the $\sigma(t\bar{t})$ method measurement. This uncertainty must be combined with the electron method scale factor uncertainty; the two should be treated as uncorrelated. The uncertainties shown below are absolute shifts.

mistag SF $\sigma(t\bar{t})$ method		HOBIT Operating Point	
source		Loose	Tight
$\sigma(t\bar{t})$	up	0.007	0.090
	down	-0.007	-0.090
luminosity	up	0.004	0.055
	down	-0.004	-0.055
jet energy scale	up	0.003	0.037
	down	-0.003	-0.037
generator	up	0.002	0.023
	down	-0.002	-0.023
ISR/FSR	up	0.000	0.005
	down	-0.000	-0.005
$t \rightarrow Wb$ branching ratio	up	0.000	0.005
	down	-0.000	-0.005
Trigger	up	0.000	0.005
	down	-0.000	-0.005
PDF	up	0.000	0.005
	down	-0.000	-0.005
W+j kfactor	up	-0.091	-0.135
	down	0.055	0.081
Statistics	up	0.024	0.125
	down	-0.024	-0.125
total	up	0.094	0.217
	down	-0.060	-0.180

Table 4: The systematic uncertainties for the b-jet tagging efficiency scale factor from the electron method measurement. This uncertainty must be combined with the $\sigma(t\bar{t})$ method scale factor uncertainty; the two should be treated as uncorrelated. The uncertainties shown below are absolute shifts.

b-eff SF electron method		HOBIT Operating Point	
source		Loose	Tight
over eff.	up	0.009	0.014
	down	-0.009	-0.014
prescale coor.	up	0.001	0.011
	down	-0.001	-0.011
Et depend.	up	0.010	0.003
	down	-0.010	-0.003
semi-lep bias	up	0.010	0.006
	down	-0.010	-0.006
charm model	up	0.001	0.002
	down	-0.001	-0.002
Stats	up	0.016	0.018
	down	-0.016	-0.018
total	up	0.023	0.026
	down	-0.023	-0.026

Table 5: The systematic uncertainties for the mistag rate scale factor from the electron method measurement. This uncertainty must be combined with the $\sigma(t\bar{t})$ method scale factor uncertainty; the two should be treated as uncorrelated. The uncertainties shown below are absolute shifts.

b-eff SF electron method		HOBIT Operating Point	
source		Loose	Tight
over eff.	up	0.024	0.092
	down	-0.024	-0.092
prescale coor.	up	0.010	0.003
	down	-0.010	-0.003
Et depend.	up	0.014	0.018
	down	-0.014	-0.018
semi-lep bias	up	0.040	0.055
	down	-0.040	-0.055
charm model	up	0.001	0.004
	down	-0.001	-0.004
Stats	up	0.078	0.163
	down	-0.078	-0.163
total	up	0.092	0.196
	down	-0.092	-0.196